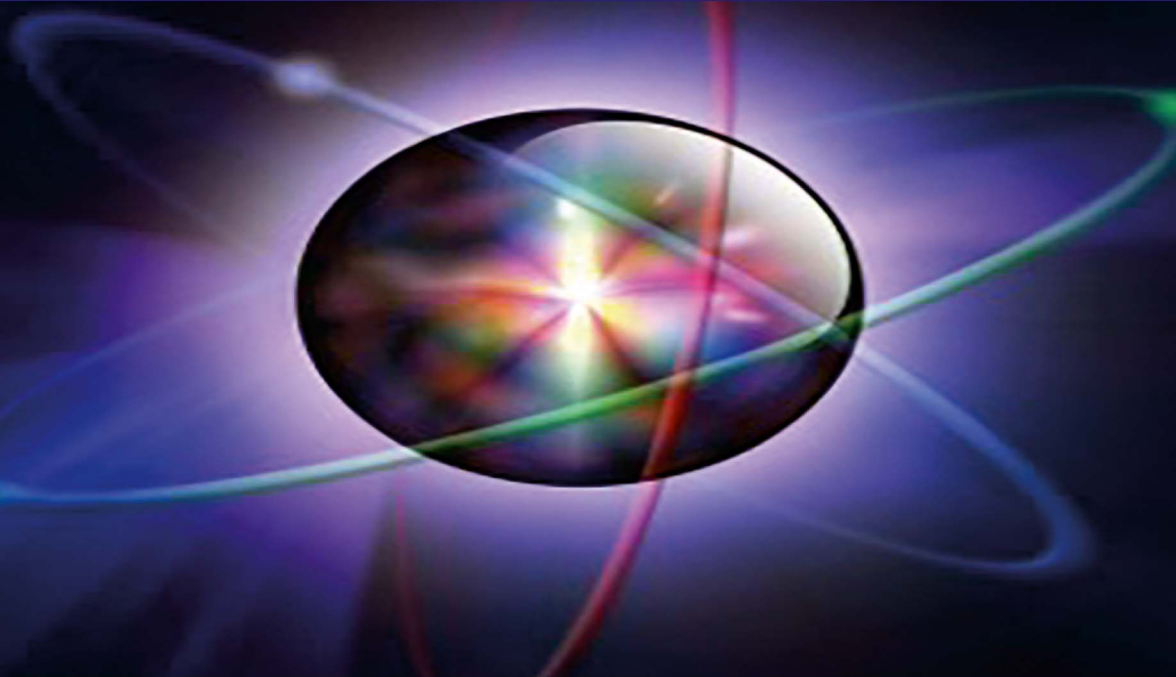# Nuclear Physics 3

*Radiopharmaceuticals
used in Nuclear Medicine*

Ibrahima Sakho

Nuclear Physics 3

*I dedicate this book to my
darling baby Mariama*

Nuclear Physics 3

Radiopharmaceuticals used in Nuclear Medicine

Ibrahima Sakho

Any opinions, findings, and conclusions or recommendations expressed in this material are those of the author(s), contributor(s) or editor(s) and do not necessarily reflect the views of ISTE Group.

Contents

Preface

Radionuclides are useful in many areas of everyday life: archaeology, biology, agronomy, medicine, industry etc. The most spectacular applications include radiochronometry (dating of archaeological objects, sediments and soils for the detection of anthropogenic pollutants, etc.) and nuclear medicine (radiopharmaceuticals used in nuclear medicine imaging, radiotherapy, etc.). The production of electrical energy in nuclear power plants exploits the properties of nuclear fission reactions. *Nuclear Physics 2* comprises four chapters devoted respectively to a description of the Big Bang model, a study of the different nucleosynthesis processes, the study of radiochronometers applied to dating and general information on radiopharmaceuticals used in nuclear medicine imaging.

This book, entitled *Nuclear Physics 3: Radiopharmaceuticals used in Nuclear Medicine*, consists of three chapters.

Chapter 1 is devoted to the study of *radiological imaging methods*. It begins with a presentation of medical imaging methods and their various medical imaging modalities. It then presents radiological imaging methods such as X-rays, γ-scan (PET) MRI scintigraphy and ultrasound. Next, photoelectric absorption, Compton effect and pair creation coefficients are introduced to express the total attenuation coefficient. The Hounsfield number is expressed as a function of the linear attenuation coefficient of water. The study then focuses on the treatment planning system (TPS), which is used to determine the dose distribution in tumors and surrounding areas during radiotherapy. Following this introduction, the principles of X-ray production, X-ray imaging and computed tomography (CT) or scanner are explained. The computer processing of elementary images to reconstruct the final image of each organ through which X-rays are passed features prominently in this section. The study then turns to nuclear magnetic resonance (NMR), explaining the principle of NMR and its physical model in biological tissues, the quantum model of Larmor precession, the phenomena of excitation and magnetic resonance, and the

quantum model of the magnetic resonance phenomenon. The study then turns to magnetic resonance imaging (MRI), with an introduction of the two MRI techniques, closed-field MRI and open-field MRI, T_1 and T_2 relaxation times, spin–lattice and spin–spin relaxation phenomena, and the phenomenon of the free induction decay (FID) signal according to an exponential in T_2^* and T_2. Following these studies, the NMR imaging sequence – which is a chronological sequence of θ-angle radiofrequency pulses and magnetic field gradients – is introduced. This enables us to study in detail the two main methods of medical imaging sequences: the spin echo sequence and the gradient echo sequence. T_1, T_2 and proton density weighting of MRI images, as well as the influence of TR repetition time and TE echo time on an NMR imaging sequence, are explained in detail in this section. This is followed by a description of slice planes, slice selection gradient, frequency encoding gradient, phase encoding gradient, Fourier plane, MRI signal decoding and the ***principle*** of three-dimensional image acquisition using a triple Fourier transform (3DFT). The chapter concludes with an explanation of the principle of ultrasound imaging and the principle of Doppler ultrasound applied to the exploration of blood flow in a vessel.

Chapter 2 is devoted to the study of *technetized radiopharmaceuticals and radiothallium-201 used in nuclear medicine*. The chapter begins with a presentation of the main characteristics of the tracers MIBI [99m]Tc (MIBI = 2-methoxy-isobutyl-isonitrile), Tetrofosmin ^{99m}Tc and ^{201}Tl used in myocardial scintigraphy. The characteristics and dosimetry of conventional gamma cameras and latest-generation CZT (Cadmium Zinc Tellurium) gamma cameras are then presented. The notions of absorbed dose (expressed in gray, symbol Gy), equivalent dose (expressed in sieverts, symbol Sv) and weighting factor (without unit) are then defined. The advantages of tracers technetized on thallium-201 are examined, as are the uses of metastable technetium-99 in scintigraphy. For each of the radiopharmaceuticals or radiotracers considered, dosimetry is presented in tabular form for the various specific organs diagnosed, and the mechanisms by which ^{99m}Tc and ^{201}Tl are excreted from the body are described. In addition, the production chains for metastable technetium-99 and radiothallium-201 are explained, as well as the relationship between effective, biological and physical half-lives, and the physico-chemical and pharmacological properties of each radiotracer. This chapter describes the principle of ^{99m}Tc MIBI and ^{99m}Tc-labelled tetrofosmin scintigraphy, and radiopharmaceuticals used to diagnose or localize myocardial infarction or myocardial ischemia. Myocardial ^{99m}Tc MIBI scintigraphy, coupled with pharmacological stimulation sensitized by Dipyridamole (Persantine®), is also described. Following on from this development, the principle of lung ventilation scintigraphy using Technetium-99m-labeled diethylenetriamine pentaacetic acid (DTPA), denoted as [^{99m}Tc]-DTPA, and the principle of lung perfusion scintigraphy using a radiotracer consisting of ^{99m}Tc-labeled human macro-albumin aggregates (MAA), denoted as ^{99m}Tc-MAA, are studied. The study then focuses on the principle of brain perfusion scintigraphy with the radiopharmaceuticals ^{99m}Tc-HMPAO

(^{99m}Tc-hexamethylpropylene-amine-oxime) and ^{99m}Tc-ECD (^{99m}Tc-ethylenediyl bis-L-cysteine-diethyl-ester), which are used for the accurate diagnosis of cognitive disorders, strokes and epilepsy. The principle of ^{201}Tl myocardial scintigraphy, used without a vector to assess coronary perfusion, is then studied. Next, the procedure for myocardial perfusion scintigraphy is described in detail, consisting of an exercise test on a bicycle (cycle ergometer) or a treadmill, or a stress test. Following on from this, the principle of bone scintigraphy using ^{99m}Tc-labeled biphosphonate carrier molecules (BPs), including ^{99m}Tc-methyl diphosphonate (^{99m}Tc-MDP) is explored. Finally, we describe the principle of static renal scintigraphy using the radiopharmaceutical ^{99m}Tc-DMSA (^{99m}Tc-dimercapto succinic acid) to assess kidney morphology, the principle of dynamic renal scintigraphy using ^{99m}Tc-MAG$_3$ (^{99m}Tc-*mercapto acetyl triglycine*) to assess kidney function and the principle of gastric scintigraphy based on the use of a standardized low-fat meal consisting of two eggs labeled with ^{99m}Tc-radiolabeled colloidal rhenium sulfide.

Chapter 3 is dedicated to the study of *the radioisotopes fluorine-18, metastable krypton-81 and iodine-123, 125 and 131 used in nuclear medicine*. It begins with a study of the physico-chemical and pharmacological properties of the radiopharmaceutical 2-deoxy-2-[^{18}F]fluoro-D-glucose or ^{18}FDG, the most widely used PET radiopharmaceutical. The process of obtaining radiofluorine-18 via the reactions ^{20}Ne (d, α)^{18}F and ^{18}O (p, n)^{18}F, the radiofluorine-18 decay scheme, the ^{18}FDG synthesis process, the principle of ^{18}FDG scintigraphy and the mechanism of ^{18}F excretion from the body are presented. Next, the physico-chemical and pharmacological properties of metastable krypton-81 (^{81m}Kr) are described, along with the ^{81m}Kr tracer production chain using the ^{81}Rb/^{81m}Kr generator and the principles of ^{81m}Kr ventilation and lung perfusion scintigraphy used without a carrier as a complement to the ^{99m}Tc-MAA perfusion test. Finally, after describing the clearance mechanism of the ^{81m}Kr tracer, the physico-chemical and pharmacological properties of [^{123}I] MIBG and [^{123}I] Ioflupane radiopharmaceuticals used in SPECT imaging for the functional study of the thyroid gland are discussed. The usefulness of iodine, the production chain of the radiotracer ^{123}I via generators ^{127}I (p, 5n) ^{123}Xe, ^{121}Sb (α, 2n) ^{123}I, ^{122}Te (d, n) ^{123}I and ^{122}Te (α, 3n) ^{123}Xe, the main emissions of the radiotracer ^{123}I, the principle of iodine-123 scintigraphy and its excretion from the body are presented. The physico-chemical and pharmacological properties of radioiodine-131 used in radiotherapy for the treatment of thyroid cancer or metastases, hyperthyroidism and goiter are then studied. This study begins with a description of the ^{131}I radiotracer production chain via the nuclear reactions ^{130}Te (n, γ) ^{131m}Te and ^{130}Te (n, γ) ^{131g}Te, the main emissions of iodine-131, the principle of iodine-131 scintigraphy and its excretion mechanism. Then, the concepts of aerosol therapy, nebulization systems, aerosol generators and median mass aerodynamic diameter (MMAD) are defined. These definitions are rounded off with a description of aerosol deposition phenomena according to their MMAD. This is followed by a presentation of the prostate in the urinary tract and prostate diseases

such as adenoma, prostatitis and cancer. These conditions are studied in detail, presenting their causes, risk factors, symptoms, diagnosis and treatment. The main treatment modalities for prostate cancer are then described. The special case of prostate brachytherapy using iodine-125 implants is examined in detail. The study begins with a description of the radioiodine-125 decay diagram, the brachytherapy modes of low-dose-rate (LDR), high-dose-rate (HDR) and pulsed-dose-rate (PDR) brachytherapy, and the procedure for brachytherapy with iodine-125 implants. Prostate chemotherapy is then briefly described.

Chapter 3 concludes with two appendices, shown in sections 3.8.1 and 3.8.2. The first appendix provides general information on strokes. This appendix provides a link between brain scintigraphy with HMPAO or ECD (discussed in section 2.5.3), which is useful for diagnosing cognitive disorders, strokes and epilepsy. In addition, this appendix is very useful for the reader, given that strokes are now known to be very frequent and constitute the leading cause of death in women and the second in men worldwide, and that 30% of stroke victims suffer from depression, according to estimates as of 2019. The second appendix is devoted to general information on thyroid and parathyroid scans, with particular reference to thyroid scintigraphy using radioiodine-123, the properties of which are studied throughout Chapter 3. This appendix is essential for understanding how the thyroid functions and the mechanism of thyroid hormone secretion that determines the various forms of hyperthyroidism (Graves' disease, basedowified goiter, hot nodules, toxic nodules, etc.). Chapter 3 is followed by a list of references, which enables the reader to deepen their knowledge surrounding the issues presented in the book. The book is completed by an index in the final section.

This book is written for students, teachers and researchers working in the fields of nuclear physics applied to medical imaging in general and nuclear medicine imaging in particular. The book is written in clear, concise language, underpinned by a highly original pedagogical style. As with the first two volumes, each chapter begins with a presentation of the general objective, the specific objectives targeted and the prerequisites necessary for understanding the chapter to be studied. In addition, corrected application exercises and a vocabulary corner defining the key concepts introduced in each paragraph are presented at various points throughout the book. This enables the reader to gain a clear understanding of the knowledge being taught, without the need for a dictionary or glossary.

This book does not attempt to cover every aspect of the description of medical imaging methods and the use of radiopharmaceuticals in nuclear medicine. However, it does provide essential information for readers working in the field of medical imaging. As human work can be perfected, we are always open to suggestions, comments or criticism from our readers that could help improve the scientific quality of this book.

Ibrahima SAKHO
Dakar
April 2024

1

Radiological Imaging

General objective	
Describe the principle of radiological imaging methods.	
Specific objectives	
Define medical imaging;	Describe closed-field MRI and open-field MRI;
Distinguish between radiological imaging and nuclear medicine imaging;	Explain the concept of spin–lattice relaxation;
Know the different medical imaging modalities;	Make the connection between longitudinal magnetization regrowth and T_1 relaxation time;
Know the nature of the radiation or fields used in medical imaging techniques;	Explain the concept of spin–spin relaxation;
Define the linear absorption coefficient;	Relate transverse magnetization decay to T_2 relaxation time after stopping a 90° pulse;
Define the intensity I (x) of a photon beam;	Interpret the evolution with time of the longitudinal and transverse components of the macroscopic magnetization vector after excitation by a 90° RF wave;
Know how the attenuation coefficient changes with atomic number Z and photon energy;	Define the notion of free induction decay (FID);
Express the relationship between the total attenuation coefficient and the coefficients of photoelectric absorption, Compton effect and pair creation;	Distinguish between spin echo and gradient echo sequences;
Define the notion of voxel;	Distinguish between echo time TE and repetition time TR;
Define the Hounsfield unit scale;	Interpret spin dephasing and rephasing phenomena during spin echo signal evolution;

Understand the usefulness of the treatment planning system (TPS) in radiotherapy;	Understand the benefits of applying a 180° pulse to overcome the inherent inhomogeneities of the instrumental magnetic field;
Describe the principle of X-ray production;	Know the intrinsic parameters of tissues that enable their characteristics to be highlighted in MRI;
Describe the principle of X-ray imaging;	Explain the principle of T_1 and T_2 image weighting and proton density;
Describe the principle of computed tomography (CT) or scanner;	Understand the influence of repetition time and echo time on the contrast of MRI images;
Explain the nuclear magnetic resonance (NMR) phenomenon;	Explain the action of MRI contrast agents to improve tissue characterization; Understand the main advantages of the gradient echo sequence;
Define the nuclear magnetic moment;	Define the notion of slice plane;
Describe the physical model of NMR in biological tissues;	Explain the usefulness of gradient slice selection;
Define the Larmor frequency in NMR;	Explain the usefulness of applying a frequency-coding gradient;
Know the order of magnitude of the resonance frequencies of the nuclei involved in NMR;	Define an NMR imaging sequence;
Know the influence of magnetic field intensity on the value of the resonance frequency for a given nucleus;	Explain the principle of eliminating residual magnetization by applying additional gradients at the end of each gradient echo cycle;
Describe the quantum model of Larmor precession;	Define the Fourier plane or k-space;
Explain the mechanism of NMR signal generation at the tissue level;	Illustrate the principle of extracting individual frequencies from a signal by applying the Fourier transform;
Define the macroscopic magnetization vector;	Understand the principle of three-dimensional image acquisition (3DFT) in MRI;
Explain the principle of tissue excitation by a radiofrequency electromagnetic wave;	Explain the principle of three-dimensional imaging using a triple Fourier transform (3DFT);
Describe the quantum model of the magnetic resonance phenomenon;	Explain the principle of ultrasound;
Distinguish T_1 and T_2 NMR relaxation times between healthy and tumor tissues;	Understand the different elements of an ultrasound scan;
Know the two magnetic resonance imaging techniques;	Explain the principle of Doppler ultrasound.
Define magnetic resonance imaging (MRI);	

Prerequisites	
Gibbs or Boltzmann–Gibbs distribution;	Radioactive decay law;
Larmor precession phenomenon;	Evolution operator;
Properties of the proton;	Zeeman Hamiltonian;
Spin magnetic moment;	Properties of ultrasonic waves;
State vector in quantum mechanics;	Doppler effect.

1.1. Radiological imaging and nuclear medicine imaging

1.1.1. *Medical imaging methods*

Medical imaging denotes all means of acquiring and reproducing images of the human body. It is used in two fundamental areas of medicine: radiology and nuclear medicine [BUV 09, ZIM 06, ANS 16, MUL 16]. The various medical imaging methods are based on different physical principles [MUL 16]:

– X-rays: radiography and computed tomography (CT);

– ultrasound;

– nuclear magnetic resonance: MRI;

– radiotracers: scintigraphy and PET (nuclear medicine).

Different types of images can be obtained by varying the type of energy used and the acquisition technology. The various ways of producing medical images are referred to as imaging modalities. Each modality has its own application in medicine [GOU 10]. The following are the different medical imaging modalities:

– transmission imaging: X-ray and computed tomography (CT) or CT scan (X-ray transmission);

– emission imaging: scintigraphy or SPECT (single-photon emission tomography (gamma photon emission)), PET (positron emission tomography), MRI (emission of radiofrequency waves in a static magnetic field);

– reflection imaging: ultrasound (ultrasonic wave reflection).

Figure 1.1 shows the different types of radiation or fields used in radiology and nuclear medicine imaging techniques.

This chapter focuses on radiological imaging methods.
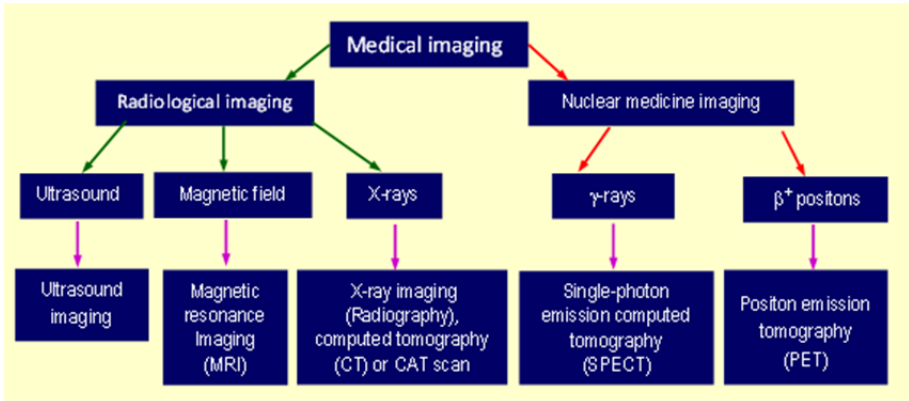
Figure 1.1. *Radiation, fields and imaging techniques*
in radiology and nuclear medicine

1.1.2. *Absorption coefficients and Hounsfield number*

Let us consider an electromagnetic beam passing through a homogeneous medium on a surface *S*. We denote by σ_e the *effective cross-section* (collision surface) of an electron and by n_e the *electron density* (number of electrons per unit volume of the medium traversed). A cylindrical beam volume with axis of revolution *Ox* therefore contains $n_e \cdot S$ electrons per unit length. By definition, the *total effective cross-section* $\sigma_t = n_e \cdot S \cdot \sigma_e$. During propagation, the beam undergoes attenuation due to absorption by the *absorbing medium*. By definition, the *linear absorption coefficient* μ is given by the relation [DIS 14]:

$$\mu = \frac{\sigma_t}{S} = n_e \cdot \sigma_e \qquad [1.1]$$

Let us denote by N_0 the initial number of photons in the electromagnetic radiation, by *N* the number of photons remaining (unabsorbed) after attenuation of the beam and by *n* the number of photons attenuated over a penetration length *x* of the beam. The fraction *dn* of photons attenuated over an elementary path *dx* is then written as:

$$\frac{dn}{n} = -\mu \, dx \qquad [1.2]$$

In equation [1.2], the sign "–" reflects the reduction in the number of photons as the beam propagates through the absorbing medium under consideration.

Integrating [1.2] between the limits N_0 and N gives the number N of photons remaining. Therefore:

$$N(x) = N_0 \, e^{-\mu x} \qquad\qquad [1.3]$$

In the case of a *heterogeneous medium* (e.g. the human body), we need to take into account the linear absorption coefficient $\mu\,(x)$ characteristic of the medium traversed (e.g. an organ) at the point of abscissa x. For an elementary path dx, equation [1.3] becomes:

$$N(x) = e^{-\int_0^x \mu(x)\,dx} \qquad\qquad [1.4]$$

By definition, the *beam intensity* $I\,(x)$ measures the energy of the radiation, or the number of photons per unit time passing through the unit area normal to the beam, at position x. According to [1.3], the intensity $I\,(x)$ of electromagnetic radiation decreases exponentially with the thickness x of the material traversed, according to the law:

$$I(x) = I_0 \, e^{-\mu x} \qquad\qquad [1.5]$$

The attenuation coefficient μ increases as a function of the atomic number Z of the atoms in the material and decreases as a function of photon energy (in this case, *X photons*). Moreover, this coefficient depends on the chemical composition of the tissues traversed. It is high for bone, medium for soft tissue and low for fat. Bone contains mineral salts (phosphorus, calcium, magnesium), which have higher atomic numbers than the main constituents of soft tissue (oxygen, carbon, hydrogen, nitrogen, etc.). They therefore absorb more *X-rays* [SAK 17].

Taking into account the heterogeneity of the biological media (bone, soft tissue, etc.) through which X-rays pass, we introduce the attenuation coefficient $\mu\,(x)$ specific to each medium. The *total attenuation coefficient* μ is the sum of three coefficients: the *photoelectric absorption coefficient* (τ); the *Compton effect coefficient* (σ); and the *pair creation coefficient* (κ). Therefore:

$$\mu = \tau + \sigma + \kappa \qquad\qquad [1.6a]$$

For X-rays, only the photoelectric absorption coefficient and the Compton effect coefficient are taken into account. Pair formation is a specific property of the gamma photon.

For a heterogeneous medium, we deduce the intensity $I(x)$ from equation [1.5]:

$$I(x) = I_0 e^{-\int \mu(x)dx} \qquad\qquad [1.6b]$$

In *radiography* or *computed tomography (CT)*, an *image* is produced by projecting a beam of X-rays through the object to be imaged. A portion of the X-ray photons is attenuated in the object, and the quantity of photons passing through it is measured by a *detector* located opposite the source. Different interactions are responsible for the attenuation of a photon beam. These interactions depend on two parameters of the material: its electronic cross-section and its electron density.

CT (*Computed Tomography*) images reflect the attenuation coefficient, which depends on electron density and effective cross-section. These two parameters are fundamental quantities for *Monte Carlo simulations* (see note at end of section). A CT device projects at different angles around an object. Upon exiting the object, the beam detected by the CT device contains all ineffective photons (those that have not interacted with the medium or have scattered to reach the device with a deviated trajectory). The CT image can be reconstructed from these projections by filtered back-projection [DIS 14].

In 3D medical imaging (scanner, NMR, PET), each elementary volume of the image is called a *voxel*. The latter is particularly well suited to the representation of a body volume made up of cross-sectional images of a patient. The cross-sectional image of an object is reconstructed from a large number of attenuation measurements at various incidences. A computer then determines the value of the attenuation coefficient μ for each voxel. The Hounsfield unit scale is a linear transformation used to determine the absorption coefficient μ in a given voxel, expressed in *Hounsfield units* (HU). The *average attenuation coefficient μ* for water is given by the following relationship [THI 07, DIS 14]:

$$HU = 1,000 \times \frac{\mu - \mu_e}{\mu_e} \qquad\qquad [1.7]$$

In equation [1.7], μ_e is the *linear attenuation coefficient* of water.

The relationship [1.7] is translated into an experimental curve. This curve is very important for systems calculating the electron density distribution of each voxel, in order to accurately calculate the delivered dose. To perform dose calculations, the value of the attenuation coefficient expressed in HU is first generally converted into electron density. The latter is typically obtained by means of a stoichiometric calibration using images of a calibration phantom. This phantom contains a series of 13 inserts in a uniform medium. The HU numbers obtained in the image are

compared with the density values of the insertions. A two-, three- or four-line regression is performed on the measurements obtained from the phantom, to form the HU–ED (Hounsfield Unit–Electron Density) curve. These lines are defined using a Matlab1 procedure developed for clinical use. This curve is then used to convert HU numbers from clinical images into electron density [DIS 14].

NOTE.–

Godfrey Newbold Hounsfield (1919–2004) was a British engineer, famous for having designed the first scanner in 1971. He built a computer that takes X-ray images of the same object from different angles, reconstructing an image of the object in slices. The application of this technique to the medical field led him to propose what we now call tomodensitometry or CT scanning. The mathematical theory behind the scanner was independently developed by South African physicist Allan MacLeod Cormack (1924–1998), who became a naturalized American citizen in 1966. Hounsfield and Cormack each received half of the 1979 Nobel Prize in Physiology and Medicine for the development of computerized tomography, known as CT scanning. The Hounsfield scale describing *radiodensity* (*opacity of a material to electromagnetic radiation in general and X-rays in particular*) and the Hounsfield unit are named in his honor.

1.1.3. *Treatment planning system (TPS)*

In *radiotherapy*, treatment preparation is carried out through a treatment planning system (TPS) to determine the *dose distribution* in the *tumor* and surrounding areas. This dose distribution must be optimized so that healthy tissue around the tumor receives the minimum dose. Many of the TPSs in use incorporate dose distribution calculation algorithms, medical image processing and tumor contouring tools.

Three fundamental points are necessary for accurate planning:

1) the use of high-quality scanned images that reliably represent the patient in the treatment position, allowing the identification of tumor structures and organs at risk. This type of imaging, thanks to image registration techniques, can be combined with other modalities such as MRI or PET;

2) precise simulation of the interaction of ionizing radiation with human tissue;

3) *dose calculation* based on the physical and geometric parameters of the treatment device and the patient.

In general, any dose planning system must satisfy a number of constraints:

– a good description of the physical processes involved in particle generation;

– patient-related heterogeneity correction with primary and secondary particle transport;

– a dose calculation at a possible random point before calculating the 3D matrix;

– on-axis dose calculation accuracy criteria for a calculation resolution of at least 5 mm < 1% and off-axis < 2%.

The quality and precision of this simulation phase is obviously linked to the accuracy of the dose calculation models and algorithms. Two main difficulties are generally encountered in dosimetric calculations with TPS: firstly, modeling the patient (a living being) with a tissue architecture that is highly complex and even virtually impossible to model completely, and secondly, treatment constraints. It is therefore necessary and essential to make approximations and optimum compromises between calculation accuracy and calculation speed.

For modeling purposes, the patient is considered as a volume made up of a set of small elements (voxels) obtained from the CT scan. As mentioned above, each voxel contains an H (Hounsfield) number representing the *attenuation of X-rays* in this volume element, and providing access to electron densities for dosimetric calculations within the voxel. Dosimetry involves calculating the physical interaction of particles with this voxel volume.

Once the patient has been modeled, the dose is calculated using models that take into account treatment parameters such as accelerator parameters (energy, collimation, intensity, etc.), as well as anatomical data. TPS currently delivers satisfactory results. However, in order to improve accuracy, and in certain situations where TPS accuracy is not sufficient, *Monte Carlo methods* may be considered. Monte Carlo simulations now represent a powerful alternative and tool for modeling dose response and calculating the corrections required for dosimetric applications. The use of these methods for complex geometries or high-resolution images requires relatively long computing times, which must be taken into account.

NOTE.–

Monte Carlo methods [ROG 82, THI 07, SPA 12, DIS 14, PET 14, DEG 17] are statistical methods based on the drawing of pseudo-random numbers, according to probability laws or probability density functions that describe natural processes (biological or physical). The name of these methods, which alludes to the games of chance played at the Monte Carlo casino (in the municipality of Monaco), was invented in 1947 by the Greek-American physicist Nicholas Constantine Metropolis (1915–1999). It was first published in 1949 in an article coauthored with the Polish

mathematician Stanisław Marcin Ulam (1909–1984). In the field of medical physics, particularly for dosimetric applications in external radiotherapy/curietherapy, Monte Carlo methods use various types of software resulting from collaborations between medical physicists and computer scientists. These methods are underpinned by several calculation codes, each specific to a given application. Examples include the *PENELOPE* (*PENetration and Energy Loss of Positrons and Electrons*) code [BAR 95] for the simulation of electron–photon cascades. This simulation is carried out in an energy range from 1 keV (100 eV for electrons and positrons) to a few hundred MeV in base materials with atomic numbers between 1 (hydrogen) and 98 (californium), as well as in compound materials. In addition, the *MCNP* (*Monte Carlo Neutron Photon*) code [BRE 00] enables the simulation of photons, neutrons, positrons and electrons. This code enables photons to be "tracked" over a wide range (from 1 keV to several GeV). This code has evolved into its new version MCNP6 following a merger of versions MCNP5 and MCNPX (*Monte Carlo N-Particle eXtended*).

VOCABULARY CORNER.–

Algorithm: the description of a sequence of steps used to obtain a result from input elements.

1.2. X-ray imaging

1.2.1. *Principle of X-ray production*

X-ray imaging uses two main instruments: an X-ray source and an X-ray detector, positioned on either side of the patient. The principle of X-ray production is illustrated in Figure 1.2 [SAK 19]. X-rays are produced in *X-ray tubes*, also known as *Coolidge tubes or hot-cathode tubes.*

Let us briefly review the principle of X-ray production.

Electrons emitted by a cathode (*a filament, usually made of tungsten, heated by the passage of an electric current*) are accelerated by a high potential difference (from 10 to 150 kV) towards a target made of a metal anode (also made of tungsten). X-rays are emitted by the target in two ways:

– The stopping of the electrons by the atoms of the target creates *continuous radiation* (*braking radiation or Bremsstrahlung*), part of which is in the X-ray range.

– The accelerated electrons have sufficient energy to excite some of the target atoms, disrupting their inner electronic layers. These excited atoms then emit X-rays as they return to their ground state.
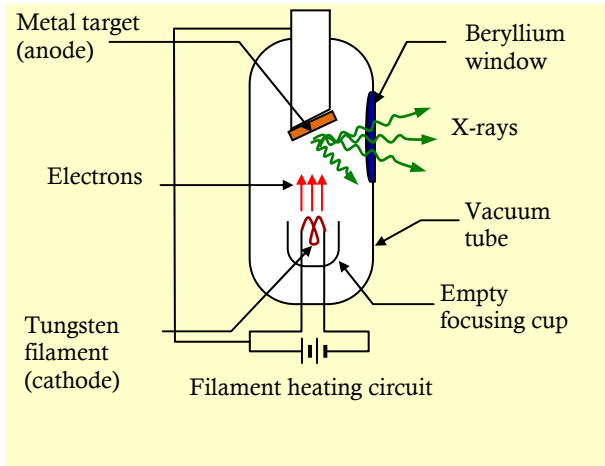
Figure 1.2. *Principle of X-ray production using a Coolidge tube. For a color version of this figure, see www.iste.co.uk/sakho/nuclearphysics3.zip*

1.2.2. *Principle of X-ray imaging*

The oldest noninvasive medical imaging technique applied to the skeleton is X-ray radiology. This early technology was born after the discovery of X-rays in 1895 by Wilhelm Roentgen, who also made the first images of human anatomy. Roentgen experimented with X-ray imaging by placing his wife Anna Bertha Ludwig's hand in the path of the X-rays. He found that the image obtained was a shadow of the hand bones, with her wedding ring visible (Figure 1.3). The bones are surrounded by a penumbra representing the flesh of the hand. The flesh is therefore more permeable to X-rays.

Roentgen's first X-ray therefore gave birth to the discipline known as radiology. Radiography is based on two main pieces of equipment: an X-ray source positioned in front of the patient and an X-ray detector (usually flat) placed on the other side (Figure 1.4).

The principle of this technique is based on the attenuation properties of X-rays by solid, liquid or gaseous materials exposed to X-ray radiation. The absorption of this radiation by the various materials through which it passes enables the formation of an X-ray image on a screen or detector.

Figure 1.3. *First X-ray image of Anna Bertha Ludwig's hand. Image taken on December 22, 1895 (source: https://en.wikipedia. org/wiki/Wilhelm_R%C3%B6ntgen)*

Figure 1.4. *X-ray equipment [ECO 13]. For a color version of this figure, see www.iste.co.uk/sakho/nuclearphysics3.zip*

Since the 1950s, X-ray imaging technology has undergone a revolution with the advent of digital technology. Unlike conventional radiology, *digital radiology* differs in its acquisition chain, which comprises a *luminance amplifier* that transforms X-rays into visible photons, and a coupling optic linked to a high-performance video camera. The video signal is digitized, visualized and stored in computer memory. It should be noted, however, that three-dimensional use of X-ray images is difficult: organs are superimposed without any indication of position other than their projection on the screen [DIL 92].

During an *X-ray examination*, X-rays are transmitted to the patient. The basic process consists of a short-duration (0.5 s) emission of X-rays from the source

positioned in front of the patient, which interacts with the patient [ECO 13]. These rays are then more or less absorbed by the biological media they pass through, with an absorption coefficient μ. The detector used then highlights the attenuation μ (x), which varies according to an exponential law taking into account photoelectric absorption and Compton scattering.

The initial homogeneous distribution of rays (those leaving the source) is modified according to the intensity with which they are absorbed (attenuated) or scattered in the body. The attenuation properties of tissues such as bone or soft tissue are different, resulting in a nonhomogeneous distribution of the rays that emerge from the patient and, consequently, reach the detector plate. In this way, the final radiographic image obtained corresponds to the image of the distribution of attenuations due to the various organs successively passed through. The detector can be either a photosensitive film or an electronic detection system (digital radiography) [ECO 13]. Figure 1.5 shows the principle of radiology acquisition. It shows white areas corresponding to highly attenuated regions (bone) and black areas (soft tissue) reflecting less attenuated areas. As the X-ray source is outside the body, this is called *transmission imaging*, where each point in the image corresponds to a piece of information along a linear trajectory through the patient's body. This type of imaging is widely used for diagnosing bone fractures, lung cancer or cardiovascular problems [ÉCO 13, POI 19].
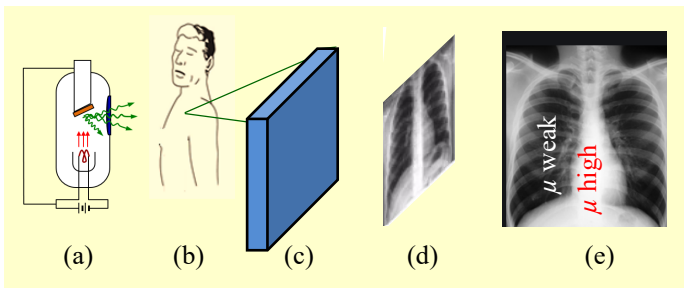

Figure 1.5. *Principle of X-ray acquisition. (a) X-ray tube, (b) patient, (c) detector + reader (conversion of X-ray photons into an image), (d) projection (of the attenuation coefficients μ of the structures crossed by the X-rays), (e) grayscale image (corresponds to the sum of the attenuations μ of the organs successively crossed. Objects appear superimposed on one another). For a color version of this figure, see www.iste.co.uk/sakho/nuclearphysics3.zip*

X-rays are also ionizing radiation, so X-ray imaging is said to be ionizing. During a radiological examination, the patient receives an equivalent dose of radiation, measured in *sieverts*. The purpose of this dose is to measure the impact of exposure to a radioactive source on biological tissues and to highlight any